Regular Article

Check for
updates

Modelling of expected B, C, N and O Lyman-α line intensities emitted from W7-X plasmas and measured by means of the W7-X light impurity monitor system

Tomasz Fornal[1,a] (iD)**, Monika Kubkowska**[1]**, Ireneusz Książek**[2]**, Dominik Stańczak**[1]**, Sławomir Jabłoński**[1]**, Rainer Burhenn**[3]**, W7-X. team**

[1] Institute of Plasma Physics and Laser Microfusion, 23 Hery Str, 01-497 Warsaw, Poland
[2] Institute of Physics, Opole University, Pl. Kopernika 11A, 45-040 Opole, Poland
[3] Max-Planck-Institut Für Plasmaphysik, Wendelsteinstrasse 1, 17491 Greifswald, Germany

Abstract The "C/O Monitor" for Wendelstein 7-X (W7-X) is a dedicated light impurity XUV spectrometer intended to measure Lyman-α transitions of hydrogen-like ions of four low-Z impurities—boron (4.9 nm), carbon (3.4 nm), nitrogen (2.5 nm) and oxygen (1.9 nm). Since the discussed diagnostic will deliver continuous information about the line intensities, it is crucial to understand the origin of the obtained signals with respect to the experimental plasma conditions (electron temperature and density). This, however, might be difficult because of the broad acceptance angle of the spectrometer and irregular shape of the plasma edge or SOL where the radiation is expected to mostly come from, depending on the plasma temperature. For that reason, numerous analyses assuming various ranges of electron density and temperature profiles of the W7-X plasmas have been performed (assuming corona equilibrium and neglecting impurity transport processes). The aim of this work is to estimate the expected radiant flux and determine the sensitivity of the system on impurity-level changes. It will allow to improve understanding between measured signal and impurity concentration.

1 Introduction

Ideal fusion plasma contains only the intended reactants, namely hydrogen isotopes and product of the fusion reaction—helium. In the real magnetic confinement fusion devices, plasma is always contaminated by some other elements so-called impurities. The origin of the contamination is usually associated with the interior of the plasma vessel—mainly the first wall materials and elements adsorbed at its surface. In some experiments, the impurities are also introduced intentionally, e.g. in order to mitigate plasma instabilities, change erosion of the wall, etc. The most unwanted impurity species are mid- and high-Z elements, which can cause essential plasma energy losses, by emission of radiation in the form of spectral lines by not fully stripped ions. Especially dangerous can be accumulation of those impurities in the central plasma region, which can lead to dilution of the fusion fuel and, in some cases, even to radiative collapse of plasma. In order to reduce these effects, the surface of plasma-facing components consists of light elements (carbon), or is covered by thin layers of low-Z

---

[a] e-mail: tomasz.fornal@ifpilm.pl (corresponding author)

Springer

elements like e.g. boron or beryllium. In modern experiments, where the material of the first wall is metallic—tungsten or tungsten-covered CFC (carbon fibre composite), the level of carbon is significantly lower but still one can observe its spectral lines. Another light element constantly observed in MCF is oxygen—this element is adsorbed in the form of water on the in-vessel surfaces during venting of the machine and then gradually released during operation of the device. The presence of nitrogen in the plasma vessel can be an indicator of leakage in the vacuum system, but in some experiments nitrogen is also introduced intentionally and afterwards it can be observed in subsequent pulses for some time.

The most useful, simple, not plasma-disturbing method of impurity study is the classical emission spectroscopy. In high plasma temperature, almost all of the atoms are stripped of electrons, and the line radiation of only highly charged ions is observed. This radiation falls in the extreme ultraviolet or X-ray range of electromagnetic spectrum. Its measurement is associated with several technical issues, e.g. low reflectivity of dispersive elements, low and not stable sensitivity of the detectors as well as problems with absolute sensitivity calibration of the system (lack of calibration sources). In the Wendelstein 7-X experiment [1], an additional difficulty is connected with planned long time of the pulse (up to 30 min) so the system needs to be protected against overheating by, for example, stray radiation.

Due to those technical difficulties (restricted number and sizes of ports), most of the spectrometers are operating along a single line-of-sight. Consequently, the measured signal is the result of integration along different plasma shells, with different temperatures, densities, and concentration of the impurity species under study. Therefore, a complex analysis has to be applied in order to derive physical quantities from measured line radiation taking into account radial temperature and density distributions and possibly even considerations on impurity transport in the plasma. Consequently, such analysis is necessary not only to get a quantitative data (as, for example, impurity concentration) but even to obtain only qualitative results (as, for example, degree of increase or decrease of impurity).

There are many diagnostic systems dedicated to the observation of contamination in the Wendelstein 7-X plasmas [2–4]. One of them will be "C/O Monitor"—the dedicated spectrometer, designed for monitoring of four main light impurities, namely oxygen, nitrogen, carbon and boron. It will be performed by registering the intensity of emission of Lyman-α spectral line of hydrogen-like ions of those elements. The exclusive purpose of this spectrometer, which is registering only the line intensities (without the study of the line shape), determines its design.

2 Spectrometer

The spectrometer is constructed based on Johann geometry with cylindrically curved dispersive elements [5, 6] for oxygen channel, it will be TlAP crystal and the remaining three channels will be equipped with multilayer mirrors. This type of geometry is associated with large acceptance angle, which increases the number of radiation quanta reaching the diagnostic system. Figure 1 presents the general geometry of the "C/O Monitor" system.

The detectors are set not tangentially to the Rowland circle but perpendicularly to the beam reflected from the crystal. This evidently distorts the line shape but provides freedom in the selection of the detector. The construction of the output arm of the spectrometer enables changes of its length in order to adjust it to different mechanical construction of the detectors, i.e. enabling to test and attach different types of detectors. Since the dynamic range of some detectors is quite low (e.g. proportional counters), a variable aperture is mounted in front of the system, which can reduce the flux of the radiation. The input aperture is of rectangular shape
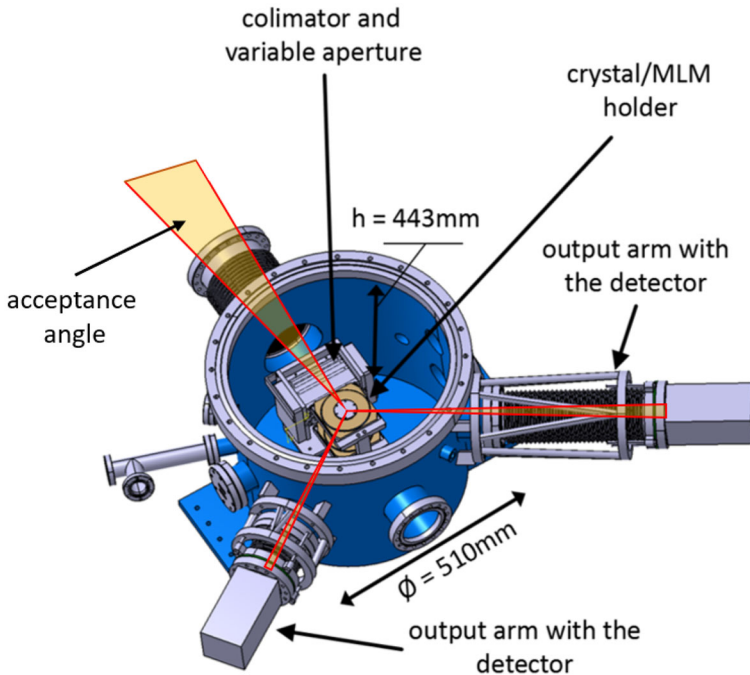
Fig. 1 Geometry of the "C/O Monitor" system

and its area can be reduced by moving a vertical diaphragm. The detailed design description of the system is presented in another paper [7]. In general, the construction is divided into two sub-spectrometers: one for measurement of carbon and oxygen line and the second one for boron and nitrogen. Each spectral line is associated with a separate measurement channel including variable aperture, dispersive element and detector. The entrance solid angle is in horizontal (dispersion) direction defined by properties of the dispersive element and its curvature, in vertical plane is set by grid collimator (individual for each channel). The line-of-sight of each channel is slightly different, but they cross each other in the vicinity of the main magnetic axis.

The peculiarities of the "C/O Monitor" construction lead to the fact that the interpretation of the registered data may be difficult. The radiation registered by the system will be emitted from quite large plasma volume stretched for approximately 10 cm vertically and several dozens of centimetres horizontally.

The motivation of the work is the qualitative determination of the trends in the behaviour of total emissivity of the selected spectral lines with respect to different possible electron temperature and density profiles of the plasmas. By means of total emissivity, here, the integral over the whole plasma volume observed by the system (radiant flux) is assumed. The outcome will help for interpretation of the experimental results registered by the "C/O Monitor".
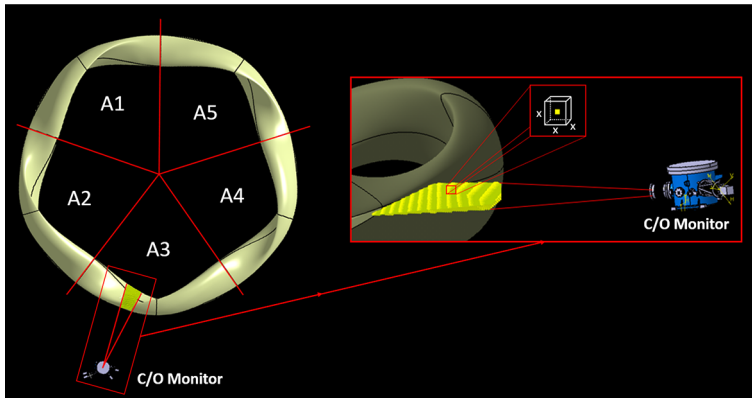
Fig. 2 Top view on the last closed flux surface of the W7-X with the "C/O Monitor" included. The zoomed part presents isometrical projection of top sub-spectrometer chamber of the "C/O Monitor" with the visualization of its acceptance angle and observed plasma volume

3 Description of the modelling method

Since the local emissivity for low-Z elements strongly depends on the n_e and T_e profiles especially at the plasma boundary, where temperatures are in the range of their maximum emission, it is important to understand the sensitivity of the radiation intensity on changes in the profiles under different plasma conditions. Such rough prediction of the emissivity changes for each element will ease an qualitative interpretation of their time behaviour during the plasma pulses in the forthcoming experimental campaign. The obtained results are strictly qualitative but ensure better understanding of the phenomena that play crucial role in the investigated low-Z elements in the W7-X plasmas.

The "C/O Monitor" system is a high-throughput device with large acceptance angle of the selected dispersive elements—even above 11° in poloidal (horizontal) plane for the O VIII Lyman-α line and approx. 1° in radial (vertical plane) for all channels. The observation of different poloidal (in horizontal direction) regions is associated with different wavelengths—according to the Johann optical set-up. We can use it, assuming that the plasma parameters are slowly changing along the main magnetic axis (in the horizontal direction).

In order to calculate the total emissivity of the investigated plasma volume, it needs to be defined in the Cartesian coordinate system using the CAD (computer-aided design) model of the diagnostics. Since for the "C/O Monitor" the observed plasma volume (defined by the acceptance angle and the lines-of-sight) is slightly different for each spectral channel, here a unified volume for all channels was used to simplify the estimation and make easier analysis of obtained results. For this purpose, the selected plasma was meshed to obtain a list of x, y, z coordinates where each represents the central point of the cubic with side length x = 1 cm and hence volume $V = 1 \text{ cm}^3$ (Fig. 2).

With the obtained matrix of plasma coordinates, the next step was to choose the specific magnetic field configuration (labelled KJM [8]) and calculate the corresponding Reff values [9] (minor effective radius) of each cube. This operation was carried out using VMEC (Variational Moments Equilibrium Code) code, dedicated to solve the magnetohydrodynamics force balance equations in a three dimensional space. The W7-X plasma shape is constructed as complex fivefold symmetric geometry (see Fig. 2) with poloidal cross sections changing from bean shape to triangle (see Fig. 3). In order to compare the plasma parameters in its
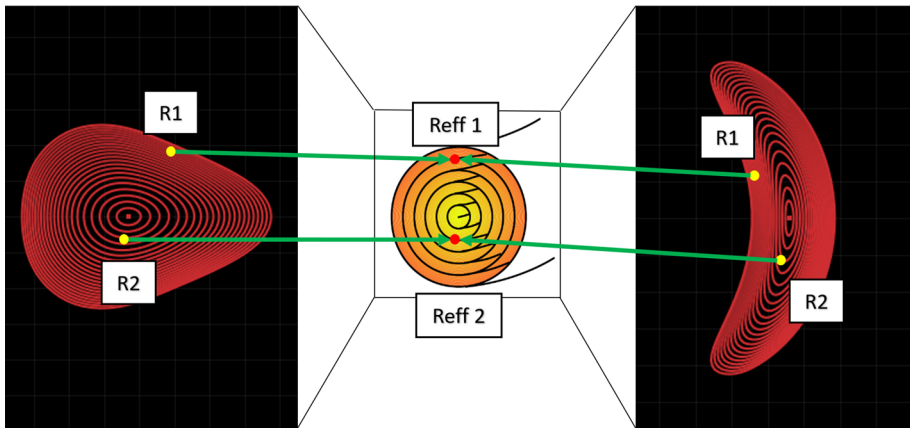
Fig. 3 Normalization of the stellarator's poloidal cross sections to the circular cross section

different regions, it is necessary to standardize the position of selected points in reference to the stellarator's magnetic axis. For this reason, the poloidally varying shapes of the stellarator's poloidal cross sections are normalized to the circular poloidal cross section (see Fig. 3), thus providing the opportunity to compare the results from different diagnostic systems at different poloidal cross sections.

Finally, with the obtained sequence of Reff values, it was possible to determine the n_e and T_e values within solid angle of the "C/O Monitor".

3.1 Temperature and density distributions used in modelling

In order to perform the modelling, two sets of experimental data were taken as examples of radial distributions of temperature and density obtained in W7-X plasmas. The first set (named scenario 1, presented in Fig. 4a) was defined based on plasma experiment 20181011_012@5_5000 characterized by a steep drop of the temperature profile in near-axis regions and semi-flat curve in the outer part. The second set of profiles (named scenario 2, Fig. 4b) based on pulse 20181016_037@3_3000 is associated with broader profiles of the plasma parameters. The effective minor radius is defined by last closed flux surface (LCFS), which is associated with magnetic field configuration. In both studied cases, the value of minor radius was equal to 0.51 m.

The profiles can be approximated by a simple analytical function—a sum of two Gaussian (Eq. 1):

$$T, N_e(R_{eff}) = A_1 \cdot exp\left(-\frac{(R_{eff} - x_1)^2}{2 \cdot w_1^2}\right) + A_2 \cdot exp\left(-\frac{(R_{eff} - x_2)^2}{2 \cdot w_2^2}\right) \qquad (1)$$

The emission of the lines under study was determined for a set of assumed T_e and n_e distributions, calculated using formula (1). For one set of data associated with a given scenario the ratio A_1/A_2 was fixed, so the shape of the distribution remains unchanged and only its values were modified. Using this method, a set of T_e and n_e distributions were calculated. The range of axis temperature as well as electron density used for this sensitivity study correspond to typical values expected in W7-X plasmas and hence represent realistic plasma scenarios/parameters. The reason for investigation of different plasma profiles is to check an
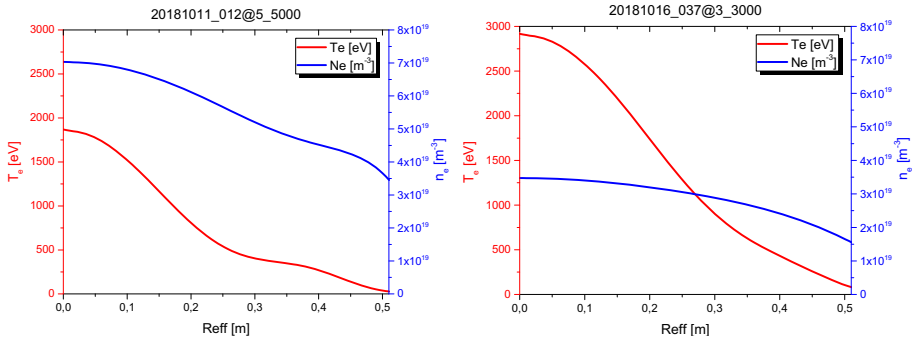
Fig. 4 Electron density and temperature profiles as a function of Reff for two plasma scenarios

Table 1 Parameters used for fitting the approximated temperature and density profiles

Approx. function parameters	A_1 [eV]	w_1 [m]	x_1 [m]	A_2 [eV]	w_2 [m]	x_2 [m]	A_1/A_2 ratio [-]
Temperature							
Scenario 1	1870	0.155	0	210	0.07	0.38	8.9
Scenario 2	2900	0.195	0	80	0.07	0.38	36.3
Approx. function parameters	A_1 [m^{-3}]	w_1 [m]	x_1 [m]	A_2 [m^{-3}]	w_2 [m]	x_2 [m]	A_1/A_2 ratio [-]
Electron density							
Scenario 1	$7.0 \cdot 10^{19}$	0.370	0	$9.8 \cdot 10^{18}$	0.11	0.50	7.1
Scenario 2	$3.5 \cdot 10^{19}$	0.400	0	$2.5 \cdot 10^{18}$	0.15	0.38	14.0
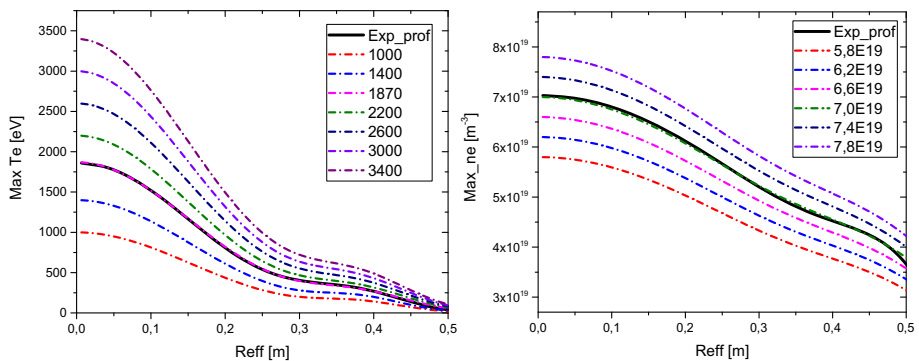
Fig. 5 T_e (left) and n_e (right) distributions approximated by a sum of two Gaussian function used for the sensitivity study

impact of the temperature/density changes on the obtained signals, while the shape of their distributions remains "unchanged".

The parameters of the approximations are listed in Table 1.

A model calculation of the set of T_e and n_e profiles representing scenario 1 is presented in Fig. 5.
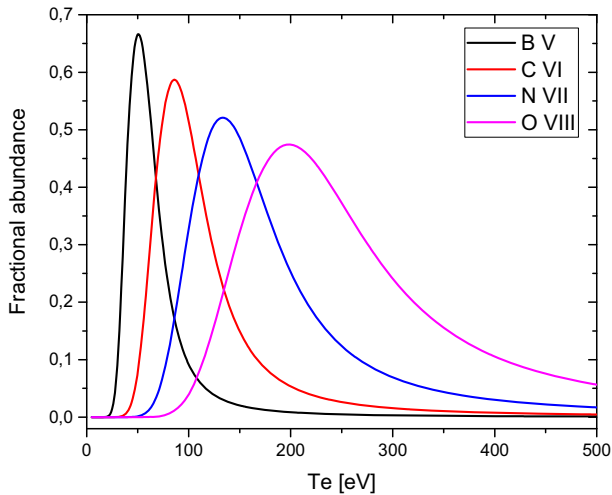
Fig. 6 Fractional abundance for hydrogen-like ions of selected impurity species as a function of electron temperature

Figure 5 presents the sample of the T_e distributions as a function of Reff (left)—the whole set contain 20 profiles with values of A1 (on-axis temperature) in the range of 1—9 keV (step 0.4 keV). Similarly, the distributions of n_e profiles in a function of Reff (right) was determined with 0.4E19 m^{-3} step in the range of A1 equal 1—9E19 m^{-3}. The same calculation procedure was performed for the second plasma scenario 2.

Such calculated set of all T_e profiles was subsequently mapped with the set of n_e distributions. This resulted in a combination of plasma parameters, what served as an input to calculate the radiation of considered Lyman-α lines. The detailed description of this calculation is presented in the next section.

3.2 Photon emissivity coefficients and fractional abundances

Using an information about the electron temperature distribution of the considered plasma volume, the respective fractional abundance (FA) values for the specific H-like ions based on the coronal balance model were calculated. Figure 6 presents fractional abundances of the representative Lyman-α transitions for investigated elements.

While the maximum of the B V line intensity and therefore the B V emission is expected at temperatures below 100 eV, the O VIII line is expected above 100 eV.

The last part required for the calculation is determination of photon emissivity coefficients (PECs) provided by the ADAS database [10]. Based on information about the local temperature, it is possible to calculate the PEC values both for excitation and for recombination radiation.

An array of designated Reff points corresponding to the n_e, T_e, PEC and FA values serves as an input to numerical code developed for numerical calculations of total emissivity estimations.
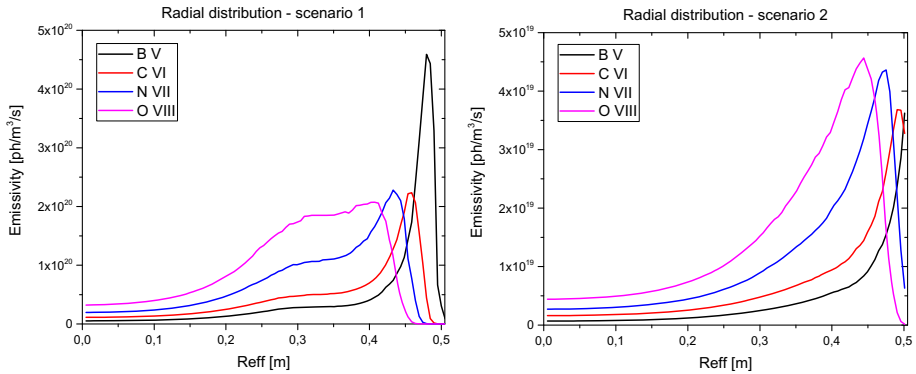
Fig. 7 Radial distribution of Lyman-α emission for scenario 1 (left) and scenario 2 (right)

3.3 Emissivity equation

The corresponding spectral emission can be obtained by formula 2 [11]:

$$I^X = \frac{n_X}{n_e} \int PEC^X(R_{eff}) \cdot n_e^2(R_{eff}) \cdot FA^X(R_{eff}) dR_{eff} \qquad (2)$$

where X—selected ion, n_X and $n_e [m^{-3}]$–impurity and electron density, $PEC^X [ph \cdot m^3 \cdot s^{-1}]$–photon emissivity coefficient and FA^X—fractional abundance under coronal ionization equilibrium, R_{eff}—minor radius [m].

Since the observed plasma volume is heterogeneous, it is represented by a set of cubes assuming 1-cm^3 volume each (as described at the beginning of this section). In order to obtain information about the requested plasma parameters (electron temperature and density) related to each mesh cube, the R_{eff} is used. Once all T_e and n_e values referring to each cube are determined, the calculation of the total intensity is performed by numerical integration of the considered plasma volume.

In the next section, the detailed description of total isotropic emission from the considered plasma volume is presented.

4 Results

To provide comparable qualitative results, the calculations were performed with an assumption of a normalized total impurity concentrations for each element equal to 2%. Since the recombination radiation has relatively insignificant contribution on the obtained results, only excitation radiation was used in the considerations. The isotropic radiation into the full solid angle was assumed here. On this basis, calculations and the qualitative analysis were performed. In order to determine the region of the plasma with the highest emissivity of selected ion, the calculation of radial distribution of investigated ions was performed. Nevertheless, one needs to keep in mind that uniform distribution of impurity is assumed. As an example, the calculations were performed for the profiles obtained during the discharges 20181011_012@5_5000 (scenario 1) and 20181016_037@3_3000 (scenario 2). The radial distribution of the emitted intensity is presented in Fig. 7.

The distribution of investigated hydrogen-like ions depends strongly on the electron temperature, especially for the element with the lowest atomic number. They exist mostly close to
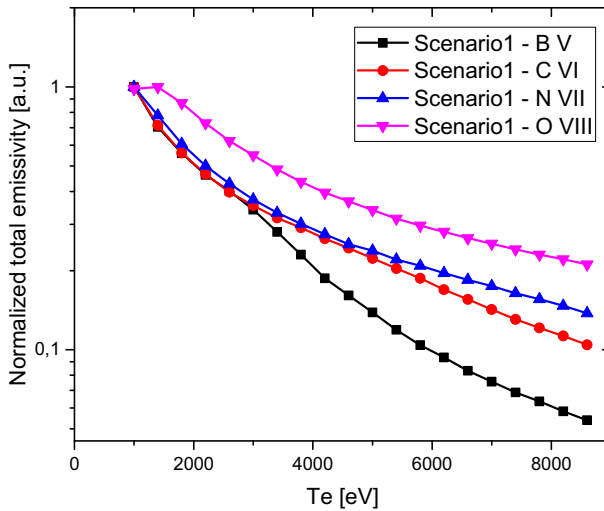
Fig. 8 Emissivity dependency on the electron temperature–plasma scenario 1

the plasma boundary, because they become fully stripped at the higher temperatures towards the interior of the plasma.

Since we might expect that the local maxima of the emitted radiations are shifted towards the plasma edge as the atomic number decreases (caused by the highest probability of ioniza-tion and excitation in the selected electron temperature), the emission value depends strictly on the electron temperature profile shapes at the plasma edge. For example, the impurities' distribution calculated for scenario 1 shows that the maximum intensity of the B V line reaches more than double intensity of other elements in the region where the temperature profile is semi-flat and reaches lower values at the edge of the plasma. On the other hand, the radial distribution of boron line for the scenario 2 shows that the total radiation emitted by line B V is significantly weaker than for other elements. The strongest part of the radiation comes directly from the last closed flux surface. This presents that the origin of the significant part of radiation fraction for boron Lyman-α might, in some scenarios, originate from the plasma layers outside of the LCFS.

The subsequent part of analysis presents the results of a mapping over the various com-binations of n_e and T_e profiles, described in Sect. 2.1. In this analysis, the total radiant flux values and the dependencies on various plasma densities and temperatures are described.

There are two major analyses where the dependencies of plasma emissivity for each investigated element with respect to the plasma scenarios were examined. The first one was performed in order to check the dependencies of total emissivity of the investigated plasma volume for each ion as a function of electron temperature. In Fig. 8, the dependency of emissivity of the electron temperature for the scenario 1 is presented. Each point on the graph represents the total emissivity for selected ions radiated from the investigated plasma volume. In order to properly compare shapes of the emissivity distributions between investigated elements, the obtained data were normalized to 1. The colours represent total emissivity of selected line, registered by the „C/O monitor for W7-X " system–black represents B V, red–C VI, blue–N VII and magenta–O VIII line emission.

For this specific plasma profiles, the decrease of B V, C VI and N VII emission is nearly identical until T_e reaches the level of approx. 3 keV. Above that temperature, the total emissiv-
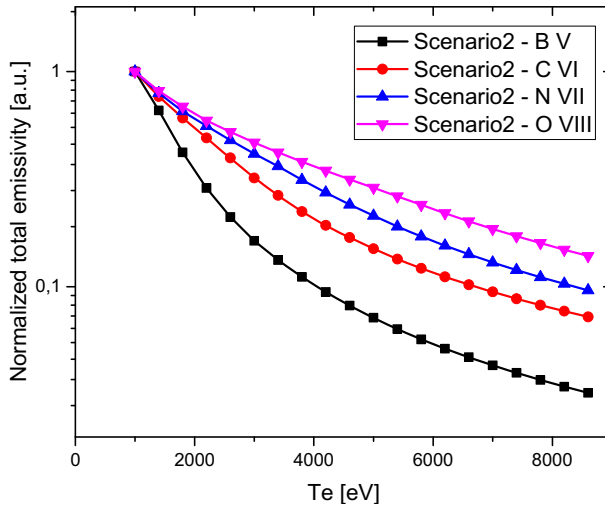
Fig. 9 Emissivity dependency on the electron temperature–plasma scenario 2

ity of the boron line significantly drops in contrast to other investigated elements. Moreover, the emissivity of the O VIII line increases slightly with rise of T_e from 1 to 1,4 keV.

In contradiction to the scenario 1, the scenario 2 (see Fig. 9) represents slightly higher electron temperature on the plasma edge. In this case, the clear dependency between the slope of the emissivity graphs corresponding to the selected elements is observed. With increase of the atomic number of impurities, the slope of the lines representing their intensity as a function of electron temperature is strongly reduced. Even small changes of T_e affect the B V signal significantly and with increase of the atomic number, the gradient of line intensities decreases gradually. The reason for the difference between the behaviour of the line emissivity for the two investigated plasma scenarios is the combination of the T_e and n_e profile shapes and absolute value of T_e at the plasma edge where the temperatures are lowest.

In order to investigate the emissivity dependence as a function of electron density for both plasma scenarios, the second analysis was performed. The study was carried out for two cases: first with assumption of high-temperature case (on-axis maximum $T_e = 8.6$ keV) and second for low-temperature case (on-axis maximum $T_e = 1$ keV).

Figure 10 presents the emissivity dependency on the electron density assuming on-axis maximum $T_e = 8.6$ keV for both plasma scenarios. Similarly, the colours represent the intensities of selected ions: black–B V, red–C VI, blue–N VII and magenta–O VIII. The solid line represents the emissivity as a function of n_e related to the scenario 1, while dotted lines illustrate the emissivity for the scenario 2. When electron temperature is 8.6 keV, the shapes of obtained electron density dependances are similar for all the elements. The values obtained for scenario 2 are always beneath the values obtained for scenario 1. The growth of all spectral line emissions is almost exponential and increases with atomic number.

However, for the same analysis but assuming low-temperature case ($T_e = 1$ keV), the distribution of total line intensities between two plasma scenarios does not follow the same rule (Fig. 11). In contrast to trends for the B V, C VI and N VII line intensities which are similar to the 8.6 keV case, for O VIII line there are very small differences in intensities obtained in scenario 1 and scenario 2 (magenta dotted and solid lines). In such case (for less energetic plasmas), the registered changes in O VIII intensities will be exclusively associated
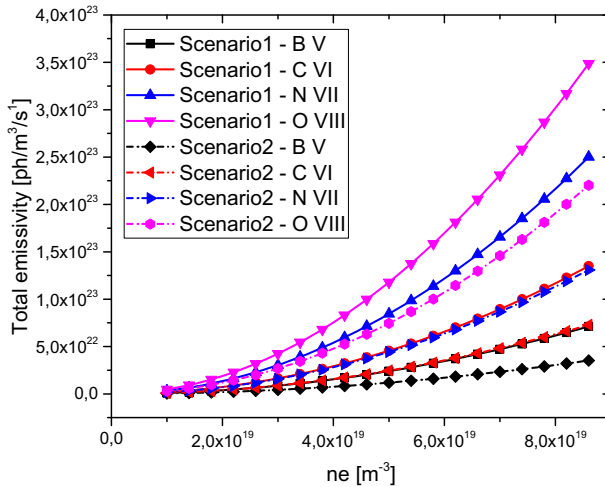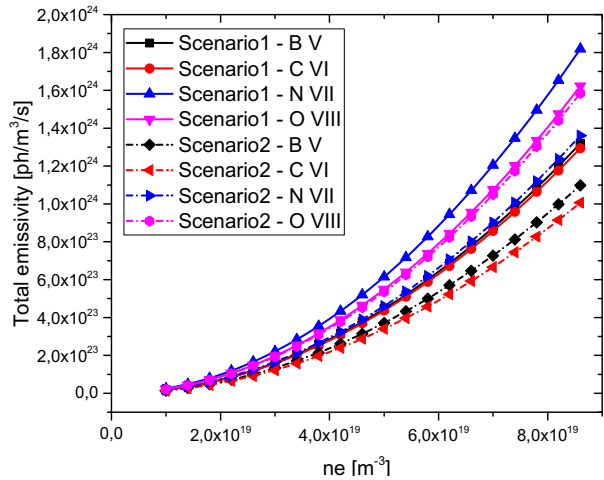
Fig. 10 Emissivity dependency on the electron density and $T_e = 8.6$ keV

Fig. 11 Emissivity dependency on the electron density and $T_e = 1$ keV

with changes of impurity concentration (not changes of temperature distribution). It can be explained by the fact that the maximum O VIII line emissivity lies in the low-temperature region, which is similar in both scenarios, where its fractional abundance reaches its maximum.

Performed analysis confirm that the various combinations of T_e and n_e profiles play a crucial role in the final result of radiated emissivity and affect the considered elements differently. The dedicated code intended for such qualitative analysis will be an important tool during an experimental campaign at W7-X, assisting in the analysis of collected data.

5 Conclusions

In order to ensure appropriate interpretation of the data registered during the forthcoming operation of the "C/O Monitor" at the Wendelstein 7-X, the series of line emissivity calculations (assuming corona equilibrium) were performed. The procedure used for the calculation of presented results will enable the quick judgement of the time behaviour of the spectral lines of the 4 elements in terms of changes in impurity concentration or just only changes in the plasma profiles. This is especially important since the "C/O Monitor" system is designed to observe large acceptance angle, and the direction of the dispersion of the system is not exactly parallel to the magnetic axis. The presented results were calculated based on the unified plasma volume in order to simplify the analysis. However, one needs to keep in mind that each energy channel will monitor slightly different plasma regions hindering the data analysis. Nevertheless, this step is planned as an extension for the future simulations. Since the performed analysis provides qualitative results, this simplified procedure is only the first step for better understanding of the future signals, which will be obtained during the "C/O Monitor" operation.

The results present the dependency of the emitted intensities for the specific impurity spectral line on the plasma parameters such as electron temperature and density. The emissivity is a complex function which strongly depends on the electron temperature and density—the higher the density, the higher the emissivity from a given plasma volume; however, an impact of the electron temperature on the signals is not so straightforward. For the B V line, the emissivity drops most drastically with increasing T_e creating the most peaked profile among the rest, higher-Z elements. The analysed data present that the trend representing total radiation emitted by the O VIII line is very weakly depended on the electron temperature and density profile/scenario. However, one needs to be aware of the fact that depending on the plasma scenario and hence the shape of the electron temperature profile (especially close to the last closed flux surface), some radiation fraction might be omitted in this modelling (but as one can see in Fig. 7 this can be important only for some cases).

References

1. R.C. Wolf et al, Nucl. Fusion **57**, 102020 (2017)
2. A. Langenberg, N.A. Pablant, T. Wegner, P. Traverso, O. Marchuk, T. Bräuer, B. Geiger, G. Fuchert, S. Bozhenkov, E. Pasch, O. Grulke, F. Kunkel, C. Killer, D. Nicolai, G. Satheeswaran, K.P. Hollfeld, B. Schweer, T. Krings, P. Drews, G. Offermanns, A. Pavone, J. Svensson, J.A. Alonso, R. Burhenn, R.C. Wolf, Rev. Sci. Instrum. **89**, 10G101 (2018)
3. M. Kubkowska, A. Czarnecka, T. Fornal, M. Gruca, S. Jabłoński, N. Krawczyk, L. Ryć, R. Burhenn, B. Buttenschön, B. Geiger, O. Grulke, A. Langenberg, O. Marchuk, K.J. McCarthy, U. Neuner, D. Nicolai, N. Pablant, B. Schweer, H. Thomsen, T. Wegner, P. Drews, K.-P. Hollfeld, C. Killer, T. Krings, G. Offermanns, G. Satheeswaran, F. Kunkel, Rev. Sci. Instrum. **89**, 10F111 (2018)
4. B. Buttenschön, R. Burhenn, M. Kubkowska, A. Czarnecka, T. Fornal, N. Krawczyk, D. Zhang, N. Pablant, A. Langenberg, P. Valson, H. Thomsen, W. Biel, and J. Aßmann, *Spectroscopic Impurity Survey in the First Operation Phase of Wendelstein 7-X* (n.d.)
5. R. Barnsley, N.J. Peacock, J. Dunn, I.M. Melnick, I.H. Coffey, J.A. Rainnie, M.R. Tarbutt, N. Nelms, Cit. Rev. Sci. Instrum **74**, 2388 (2003)
6. P. Beiersdorfer, S. Von Goeler, M. Bitter, K.W. Hill, R.A. Hulse, and R.S. Walling, *High-Resolution Bent-Crystal Spectrometer for the Ultra-Soft X-Ray Region* (n.d.)
7. T. Fornal, I. Ksiazek, J. Kaczmarczyk, W. Figacz, M. Kubkowska, R. Burhenn, F. Kunkel, R. Laube, and S. Renard, Rev. Sci. Instrum. (2019)
8. J. Geiger, C.D. Beidler, Y. Feng, H. Maaßberg, N.B. Marushchenko, and Y. Turkin, Plasma Phys. Control. Fusion **57**, (2015)
9. B.P. Van, A.L. Fraguas, and J. Geiger, 1 (n.d.)
10. Summers, H. P. ADAS User Manual, Version 2.6 http://www.adas.ac.uk (n.d.)
11. T. Nakano, A.E. Shumack, C.F. Maggi, M. Reinke, K.D. Lawson, T. Pütterich, S. Brezinsek, B. Lipschultz, G. Matthews, M. Chernyshova, K. Jakubowska, M. Scholz, J. Rzadkiewicz, T. Czarski, W. Dominik, G. Kasprowicz, K. Pozniak, W. Zabolotny, and K.D. Zastrow, in *41st EPS Conf. Plasma Physics, EPS 2014* (2014)